Integrated Drought Evaluation Index: Considering The Feedback of The Soil Ecological Environment on Wheat

Yanbin Li
North China University of Water Resources and Electric Power
Yuexiong Wang (w1839881@sina.com)
North China University of Water Resources and Electric Power https://orcid.org/0000-0001-9657-476X
Daoxi Li
North China University of Water Resources and Electric Power
Jiawei Guo
North China University of Water Resources and Electric Power
Xuefang Du
North China University of Water Resources and Electric Power
xiaodong Wang
North China University of Water Resources and Electric Power

Research Article

Keywords: Integrated evaluation, Ecological drought, Natural disaster risk management, Soil moisture environment, Remote sensing

Posted Date: June 9th, 2021

DOI: https://doi.org/10.21203/rs.3.rs-587363/v1

Integrated drought evaluation index: Considering the feedback of the soil ecological environment on wheat

Journal

NATURAL HAZARDS

Author names

Yanbin Li [1], Yuexiong Wang [1, *], Daoxi Li [1], Jiawei Guo [1], Xuefang Du [1], Xiaodong Wang [1]

Affiliations

1 College of Water Conservancy, North China University of Water Resources and Electric Power, Henan, Zhengzhou 450046, China;

E-mail: Liyb101@sina.com (Y.L.), w1839881@sina.com (Y.W.), ldx97042@163.com (D.L.), jiaweimartinguo@126.com (J.G.), 928101510@qq.com (X.D.), wangxiaodong@ncwu.edu.cn(X.W)

Corresponding author

* Corresponding Author

E-mail: w1839881@sina.com (Y.W.);

Tel.: +86-1833-235-9881;

Acknowledgments

We acknowledge the data support provided by the National Earth System Science Data Center of the National Science & Technology Infrastructure of China (http://www.geodata.cn). We also appreciate NASA, the Chinese Academy of Sciences and the National Meteorological Information Center for providing satellite and meteorological data to help complete this research.

Abstract

With the acceleration of climate instability, drought is causing increasing losses that seriously threaten food security in China. In consideration of the feedback of the ecological environment vulnerability on drought, this study selects the temperature vegetation dryness index to evaluate the boundaries of the regional ecological drought index and integrates many factors, such as precipitation, temperature and human activities, from the four aspects of natural disaster risk management — hazard, vulnerability, exposure and resistance—to establish an integrated drought evaluation index for wheat (IDEIW). The results showed that drought was the main reason for the observed decrease in wheat production of Anyang city, as the most severe water shortages occurred during the physiological water demand period of wheat from March to May. Precipitation scarcities were concentrated throughout the north of the study region, where drought was most frequent and severe. There were highly positive spatial correlations between the IDEIW and the annual yield reduction rate of wheat in dry years, whose bivariate Moran's I values reached 0.39, 0.42, 0.31 and 0.38 in the 2002, 2005, 2011 and 2016, respectively; further, the yield reduction rate increased with drought aggregation. This study clearly demonstrates that, in terms of availability, precision and sensitivity, the IDEIW, which is stronger and stabilizing than the temperature vegetation dryness index and the standardized precipitation index, can be used as an important tool to assess and monitor dynamic variations in agricultural drought and provide a new means for the early warning and forecast management of agricultural drought.

Keywords: Integrated evaluation; Ecological drought; Natural disaster risk management; Soil

moisture environment; Remote sensing

1 Introduction

The 6th meeting of the Intergovernmental Panel on Climate Change **(IPCC 2018)** pointed out that, with the environment experiencing global warming, extreme weather will become more difficult to determine, especially drought, will occur increasingly frequently. According to incomplete statistics, from 2004 to 2015, the average annual loss of China's grain caused by drought reached 64.07 billion yuan (**Qu et al. 2019**), indicating that drought has become the main threat to food production security in China.

At present, studies in the field of drought have made great achievements. The single-factor evaluation approach is commonly used in these studies; these single factors include meteorological drought indicators such as the standardized precipitation index (SPI) and standardized precipitation evapotranspiration index (SPEI) as well as socioeconomic drought indicators (**McKee et al. 1995; Vicente-Serrano et al. 2012; Mehran et al. 2015**). The temporal and spatial evolution characteristics of southern China have been discussed using SPI to calculate the drought intensities and variation trend rates (**Huang et al. 2010**). However, drought events result from complex effects. Human activities exacerbate nonstationary variations in drought (**Wen et al. 2020**), and single-factor studies must inevitably conceal the effects of some factors on drought intensities, causing inaccurate identifications of drought trends (**Kumar et al. 2021**). Therefore, it is necessary to build an integrated evaluation approach to objectively analyze drought characteristics. According to the theory of natural disaster risk management (**Okada et al. 2004**), the damage process of disasters mainly includes the hazard of the disaster-causing factors, the vulnerability of carriers and the degree of exposure. According to natural and man-made attributes, vulnerability is also classified

as the sensitivity and resistance of carriers to disasters (**Zhang et al. 2006**). The necessity of integrated evaluations was proven when analyzing agricultural drought in the Aharchay River Basin (**Karamouz et al. 2013**). Certain limitations exist when using SPI and other conventional indicators to identify drought intensities, especially in cases of human activities affecting water quality.

However, little attention has been given to the relationship between drought and the ecological environment in drought-stricken regions in past studies. Even if there is no human interference, a drought will occur may be based on that the ecosystem exceeds its carrying capacity (**Crausbay et al. 2017**). The destruction of ecological balance is not only detrimental to the growth of crops but also increases the frequency of drought (**Wilson et al. 2018**). Such feedback is not easily detected. Seo-Yeon *et al*. (**2020**) used the dynamic balance between dominant species and endangered species in the Gam River Basin to analyze the ecological problems caused by long-term meteorological drought. However, the influence of ecological factors on the quality of soil organic matter in drought-plagued regions has long-term effects (**Wang et al. 2013**), so one study alone is not of great significance. Vegetation types and biomass were used to establish an integrated drought evaluation system in Inner Mongolia (**Zhang et al. 2019**) with the hope of reflecting the drought-resistant ability of the ecosystem through the use of the normalized difference vegetation index (NDVI). However, the NDVI can only explain ecological conditions through vegetation coverage in a certain period of time, while the temperature vegetation dryness index (TVDI) can reflect the soil moisture environment with better effects (**Xia et al. 2020**). In this study, the TVDI was adopted to reflect drought and ecological effects, and an integrated evaluation model was

established based on the theory of natural disaster risk management. Moreover, the temporal and spatial distribution characteristics of drought in Anyang city, Henan Province were used to verify the reliability of the integrated model and provide a theoretical basis for drought assessments in this district.

2 Materials and methods

2.1 The study area

Anyang city is located in the northernmost district of Henan Province; there are many meteorological observation stations surrounding this region with relatively complete data series. The topography of the region is generally high in the west and low in the east, with the Taihang Mountains located in western Anyang city. Therefore, crops are mainly planted in eastern Anyang County (Figure 1). Wheat is the main grain crop grown in this city in summer. With superior topographic conditions, Anyang city bears the heavy responsibility of fundamental grain production in Henan Province, with an average annual planting area of more than 4.5 million mu (**Zhang et al. 2011**); Hua County was the first large wheat-producing county in northern Henan.

However, the spatial and temporal distributions of precipitation in Anyang city are uneven, with very little precipitation occurring in spring and summer. The planting time of wheat in this region lasts from October of a given year to June of the next year, and the water demand period lasts from the jointing period to the heading period, coinciding with the dry period in this region, severely threatening the growth of wheat. Two severe droughts occurred from 2008 to 2011 alone.

Therefore, taking Anyang city as an example, establishing an integrated evaluation model is of certain theoretical and practical significance to explore the distribution rule of drought and to realize dynamic monitoring of drought trends.

2.2 Data sources and processing

In this study, satellite data, statistical data and meteorological data of Anyang city covering the last 30 years (1989-2018) were collected. Since from March to June is the physiological water demand period of wheat in Anyang city, the data of these months were selected for analysis. To directly reflect the variation in the spatiotemporal characteristics of drought, the spatial interpolation or raster overlay approach was used to obtain the spatial distribution of drought.

2.2.1 Satellite data

The satellite data used in this study mainly comprise Landsat data and nighttime light data sets (http://satsee.radi.ac.cn/cfimage). The multiple cropping index (MCI) is the ratio of the actual crop planting area to the arable land area, reflecting the impact of crop planting times on the loss due to drought; these values were obtained from the National Earth System Science Data Center of the National Science & Technology Infrastructure of China (http://www.geodata.cn). The Landsat data provided by NASA had a high spatial resolution of 30 m; these data are more accurate than MODIS (Moderate-resolution Imaging Spectroradiometer) and are usually used to retrieve land surface temperatures (**Song et al. 2015**). By means of curve fitting, the relationship between the light value and the population of each township was established by using the nighttime light data, and the

spatial distribution of the population density was obtained by an inversion method applied to this relationship.

The temperature vegetation dryness index (TVDI) was proposed to consider the effects of vegetation and land surface temperature (**Sandholt et al. 2002**). The TVDI can reflect the soil moisture content of the 10-20 cm layer well (**Wang et al. 2009**). The higher the land surface temperature is, the lower the soil moisture content is and the higher the TVDI value is. Excessive surface evaporation increases the probability and intensity of drought (**Guo et al.2015**) and can even cause the destruction of the ecological balance, thus affecting the wheat yield. The formula used to calculate TVDI is as follows:

$$TVDI = \frac{LST_{max} - LST_i}{LST_{max} - LST_{min}} \quad (1)$$

Among which $LST_{max} = a_1 + b_1 \times NDVI_i$; and

$LST_{min} = a_2 + b_2 \times NDVI_i$.

where LST_{max} and LST_{min} are the maximum and minimum land surface temperatures in the same vegetation index pixel, respectively, and represent the dry and wet edges of the $LST \sim NDVI$ feature space; LST_i is the surface temperature value of any pixel; a_1, b_1, a_2, b_2 are the fitting coefficients of the dry edge and wet edge; and $NDVI_i$ is the normalized difference vegetation index of any pixel.

2.2.2 Statistical data

The statistical data were obtained from Anyang city's Statistical Annual yearbook and included the population density (POP), wheat yield, crop coefficient and so on. According to the wheat

planting area and crop planting area, the proportion of the wheat planting area in each county (WPP) could be calculated. In this study, the annual wheat yield was calculated by the sliding trend approach to obtain the annual yield reduction rate (YRR) to remove the impact of modern agricultural technology on the yield values. The calculation steps are as follows Wu *et al.* (**2021**).

The first step is the additive decomposition process of the output:

$$Y = Y_w + Y_t + \Delta Y \quad (2)$$

where $Y(\mathrm{kg/hm^2})$ is the actual wheat yield; $Y_w(\mathrm{kg/hm^2})$ is the meteorological yield of wheat affected by fluctuations in climatic elements; and Y_t（$\mathrm{kg/hm^2}$）is the wheat yield trend, which represents the natural fluctuation of the wheat yield due to the limited influence of scientific and technological progress in adjacent years. The term $\Delta Y(\mathrm{kg/hm^2})$ represents the random yield. Increases and decreases in wheat are rarely caused by regional mutations and are affected by the long-term effects of certain factors; thus, ΔY is generally considered to be zero.

The second step is to calculate the wheat yield trend:

$$Y_i = a_i + b_i t \quad (i = 1,2,3 \ldots n - K + 1) \quad (3)$$

where i represents the sequence number of the equation; K is the sliding step size (K = 11 in this study); N is the number of samples (N = 30 in this study); $Y_i(\mathrm{kg/hm^2})$ is the wheat yield trend in the ith year; and t is the time sequence number (when $i = 1, t = 1, 2, 3 \ldots \mathrm{K}$; when $i = \mathrm{n} - \mathrm{k} + 1, \mathrm{t} = \mathrm{n} - \mathrm{k} + 1, \mathrm{n} - \mathrm{k} + 2, \mathrm{n} - \mathrm{k} + 3 \ldots \mathrm{N}$).

The third step is to remove the difference of fluctuations using the multiyear average:

$$\bar{Y}(t) = \frac{1}{q}\sum_{j=1}^{q} Y_j(t) \quad (4)$$

where $\bar{Y}(t)(\mathrm{kg/hm^2})$ represents the average trend production of year t; j represents the sequence number of each time sequence equation calculation; and q is the total number of calculations for each time series equation and is related to N and K ($q = 6$ in this study).

The fourth step is to calculate the annual reduction rate:

$$YRR = \frac{Y - Y_t}{Y_t} \quad (5)$$

where $YRR(\%)$ is the annual wheat yield reduction rate. The YRR was used to represent the degree of disaster in this study.

2.2.3 Meteorological data

Agricultural drought occurs on the premise that an imbalance of precipitation and evaporation in a given region leads to insufficient water, making it difficult to meet the needs of crop growth. In this study, meteorological data and gridded data sets from 1989 to 2018 were downloaded from the China Meteorological Data Service Center (http://data.cma.cn/). The meteorological data mainly included precipitation, temperature, wind speed and sunshine duration data. Ordinary Kriging Interpolation was used to obtain raster precipitation and temperature data with a high spatial resolution of 30 m to unify the spatial resolutions of various data sets. The crop water deficit anomaly index (CWDIa) is an agricultural drought index that is based on the principle of field water balance and reflects the water demands of wheat at different physiological stages by using potential evaporation and crop coefficients. The CWDIa was obtained by sunlight and air temperature through the Penman-Monteith formula, and the specific formula is as follows (**Allan**

et al.1998; **Wei et al. 2019**):

$$CWDIa = \begin{cases} (CWDI - \overline{CWDI}) \Big/ (100 - \overline{CWDI}) & (\overline{CWDI} > 0); \\ CWDI & (\overline{CWDI} \le 0); \end{cases} \quad (6)$$

$$CWDI = a * CWDI_j + b * CWDI_{j-1} + c * CWDI_{j-2} + d * CWDI_{j-3} + e * CWDI_{j-4} + f * CWDI_{j-5}; \quad (7)$$

Among which $\overline{\mathrm{CWDI}} = \frac{1}{n}\sum_{i=1}^{n} CWDI_i$;

$CWDI_j = \left(1 - P_j \Big/ (K_c ET_0)\right)$,

Where $CWDIa$ is the crop water deficit anomaly index; $CWDI$ is the crop water deficit index; $\overline{CWDI}$ is the crop water deficit index multi-year average; a, b, c, d, e and f are the equation coefficient; j is the period of calculation; i is the sequence number of the equation; P_j is the precipitation; K_c is the Crop coefficients; and ET_0 is the potential evaporation.

The annual precipitation variability is close to the gamma probability distribution function, and the standardized precipitation index (SPI) can be obtained by standardizing the rainfall by conforming the series to the skewness distribution to indicate the occurrence probability of precipitation in a certain period of time. Assuming that the precipitation in a certain period is χ, then the probability function of its gamma distribution is as follows (**McKee et al. 1995**):

$$G(\chi) = \frac{1}{\beta^{\alpha}\Gamma(\alpha)} \chi^{\alpha-1} e^{-\frac{\chi}{\beta}} \quad (\chi > 0) \quad (8)$$

Among which $\Gamma(\alpha) = \int_0^{\infty} \chi^{\alpha-1} e^{-\chi}\, d\chi$,

where α is the shape parameter; β is the scale parameter; χ is rainfall; and $\Gamma(\alpha)$ denotes the gamma function. The maximum likelihood approach is used to estimate the optimal gamma

distribution parameters α and β as follows:

$$\hat{\alpha} = \frac{1}{4A}\left(1 + \sqrt{1 + \frac{4A}{3}}\right) \qquad \hat{\beta} = \frac{\bar{\chi}}{\hat{\alpha}} \tag{9}$$

where $A = \ln(\bar{\chi}) - [\sum \frac{\ln(\chi)}{n}]$ and n is the length of the calculated sequence.

After that, the cumulative probability function $G(\chi)$ is obtained by the integral gamma function. Since the gamma function is not defined at x=0, if the precipitation is zero, the cumulative probability function becomes the following expression:

$$H(\chi) = q + (1 - q)G(\chi) \tag{10}$$

where Q is the probability of a zero occurring in the precipitation series. Finally, the SPI is obtained after standardization.

Due to the different emphases of SPI at different time scales with different adaptabilities (**Xu et al. 2020**), a serviceability test (Table 1) was carried out for four monthly scales, and SPI6 was finally selected as the precipitation indicator in this study.

Generally, the probability of drought, which is equal between wet and drought, varies with the degree of drought (**Li et al. 2021**). Mild drought and moderate drought accounted for 34.1 % and 9.2 %, respectively. The probability of severe drought was only 4.4 %, and the extreme drought was with the level of only 2.3%, leading to the phenomenon of large-scale total crop failure. The division range of each index was determined by the probability of drought (Tab 2).

2.3 Model building

2.3.1 Principle of indicator selection

238 The factors influencing the drought evaluation results mainly include the meteorological
239 conditions, water demands of crops, growing environments and human activities (**Lu et al. 2015;**
240 **Huang et al. 2009; Zhao et al. 2016**). It is generally believed that a lack of precipitation that
241 cannot meet the normal needs of crop growth is the main cause of drought, that is, the drought
242 hazard. Water produced by precipitation is seldom directly absorbed or utilized by crops; generally,
243 soil water is absorbed by wheat roots to meet physiological needs by replenishing water sources
244 and creating an excellent growth environment after precipitation (**Yao et al. 2012**). Vulnerability
245 refers to the sensitivity of crops to disasters and reflects the stability of the growing environments
246 of crops. However, due to climate restrictions in northern China and excessive human exploitation
247 and abuse, ecological deterioration has reduced the ability of the environment to resist drought
248 (**Pei et al. 2013**) and has increased the vulnerability of the carrier, causing drought to be more
249 likely to occur (**Wang et al. 2010**). In a similar way, human activities such as man-made variations
250 in the wheat planting ratio to increase exposure will also interfere with drought intensity. Therefore,
251 in this study, SPI and CWDIa were selected as the hazard assessment indexes, POP, WPP and MCI
252 were used to reflect the effects of human activities on drought, and TVDI was used as a
253 vulnerability index to evaluate the stability of the studied soil ecosystem. These indicators can be
254 integrated into a new evaluation model using the theory of natural disaster risk management.
255
256 *2.3.2 P-value results among indicators*
257 Pearson correlation was used to analyze the degree of correlation among various indicators, and
258 the P value of the correlation coefficient was calculated to check the overlaps of selected indicators

and to screen repeated items. When calculated for the same factor, these two indicators have obvious correlations (**Raheem et al. 2019**). The results (Table 3) show that all the correlation coefficients fail to pass the significance test, while many shows relatively close relationships. That is, the correlations between these indicators are not obvious, indicating that the selected indicators are independent of each other and that the effects on disaster are not in the same direction. Therefore, it is feasible to use these indicators to build the integrated evaluation model.

2.3.3 Construction of integrated evaluation model

In this study, AHP was used to determine the weight of each index (Table 4), and the influence of the intermediate mechanism on the results was offset by appropriately amplifying the proportion of the hazard assessment index and reducing the proportion of the vulnerability assessment index in the integrated model. To facilitate this calculation, the principle of standardization was used to eliminate the differences among the data units. In this integrated model, precipitation and multiple cropping times are not conducive to drought, while the drought intensity is expected to increase with increases in the other indexes; thus, different processing approaches should be adopted for positive and negative indexes (**Galarça et al. 2010**).

For positive indicators, the following processing approach is adopted:

$$x_{st} = \frac{x_i - x_{min}}{x_{max} - x_{min}} \quad (11)$$

while for negative indicators, the following processing approach is adopted:

$$x_{st} = \frac{x_{max} - x_i}{x_{max} - x_{min}} \quad (12)$$

where x_{st} is the result after standardization, and its value ranges from [0,1]; x_{max} is the

maximum value of the processing index; x_{min} is the minimum value existing in the processing index; and x_i is any value of the processing index.

Considering the interactions among the precipitation supply, water demand of wheat and environmental resistance, the integrated drought evaluation index for wheat (IDEIW) was constructed based on natural disaster risk management:

$$IDEIW = a * SPI_{st} + b * CWDIa_{st} + c * TVDI_{st} + d * POP_{st} + e * WPP_{st} + f * MCI_{st};$$

where a, b, c, d, e and f are the weights of each component index in the integrated evaluation model; and SPI_{st}, $CWDIa_{st}$, $TVDI_{st}$, POP_{st}, WPP_{st} and MCI_{st} are the new indexes of SPI, $CWDIa$, $TVDI$, POP, WPP and MCI after standardization.

The IDEIW reflects the intensity of drought in the drought-plagued regions, and the higher the value is, the more severe the drought is. Its value ranges from [0,1], and the classification standard is determined by the occurrence probability of all levels of drought (**Li et al. 2021**), which include wet spells (0.0 < IDEIW≤0.50), mild drought (0.50 < IDEIW≤0.80), moderate drought (0.80 < IDEIW≤0.90), severe drought (0.90 < IDEIW≤0.96) and extreme drought (0.96 < IDEIW < 1.0).

3 Results

3.1 Temporal variability in precipitation

Using the meteorological data collected at Anyang Station from 1989 to 2018, the annual and monthly mean values and precipitation deviations were calculated based on the average annual

precipitation. The results show that in terms of monthly variation, precipitation presents seasonal characteristics (Figure 2): in autumn and winter, the curve is above the horizontal axis, and there is sufficient water; however, in spring and summer, the precipitation index is negative (from March to June), and the studied region is relatively dry. Studies have shown (**Zhang et al. 2016**) that if there is continuous rainless weather, the amount of stored water is not enough to compensate for the vacancy, and the potential for drought is high; this is also an important reason for the frequent droughts observed in Anyang city.

In terms of the variation in the annual sequence, the amplitude of the precipitation fluctuation is large (Figure 3), and a large negative deviation is observed every four years. The first deviation occurred in 1995, when there was almost no precipitation over the whole year, resulting in two years of continuous losses in wheat production. The rainfall in 1998, though very abundant, also reduced wheat production. Then, from 1999 to 2001, a continuous drying regime caused an increase in the wheat yield reduction rate. From 2010-2014 and in 2016, severe water shortages also led to declines in production. In conclusion, the wheat yield in Anyang city is mainly affected by drought, and drought usually occurs with a decrease in precipitation.

3.2 Spatial relationship between TVDI and YRR

The level of the annual wheat yield reduction rate reflects the degree of drought (**Chen et al. 2018**). In this study, the bivariate Moran's Index (Moran's I) was selected as the spatial correlation analysis approach. Compared with the conventional analysis approach, Moran's I reflects the potential spatial dependence of two variables (**Anselin 1995**). The larger the absolute value of

322 Moran's I is, the stronger the dependence is and the greater the correlation is. If Moran's I is positive,
323 it indicates a positive spatial correlation, meaning that the wheat yield is more serious in regions
324 with low soil moisture contents. If Moran's I is negative, it indicates the opposite situation. The
325 bivariate Moran's I is composed of the univariate Moran index and the Pearson correlation
326 coefficient. See Li *et al.* (**2017**) for the specific calculation formula.

327 The distribution results of the TVDI showed that in the early stage of water demand for
328 crop growth, drought first appeared in the central and eastern districts of the study areas (Figure
329 4a); then, disasters gradually appeared in the western districts of the study areas (Figure 4b and c).
330 The TVDI and YRR were roughly positively correlated in space, that is, TVDI and YRR varied in
331 the same direction; the higher the Moran's I value was, the more severe the YRR and the more
332 severe the drought was, which is consistent with the results of Liu *et al* (**2018**). In 2002 and 2016,
333 the Moran's I values were greater than 0.30, showing a slightly strong spatial correlation (Figure
334 5a and d). However, in 2011, Moran's I was only 0.16 (Figure 5c), and this relationship was not
335 obvious (P value =0.106). The result of the 2005 evaluation was also not within the ideal range
336 (Figure 5b). This result indicated that the applicable conditions of the TVDI were limited to some
337 extent, and the evaluation precision was insufficient, especially for the monitoring of long time
338 series-scale drought.

339

340 ***3.3 Spatial analysis of precipitation***

341 At present, the SPI is widely used in drought assessment. The SPI and SPEI were compared with
342 the variations in precipitation and drought in Iran (**Sharafati et al. 2020**), and it was believed that

there was no difference in the analysis results of the two indexes, so the spatial distribution of the SPI could represent the spatial variation in precipitation well. The results of this study show that precipitation in most regions is extremely scarce except in the western hilly region (Figure 4e-f) because the Taihang Mountains in western Anyang city block low-pressure cold air coming from the northwest, which is consistent with the results of Liu *et al* (**1999**). The water shortages in northeastern Anyang city were relieved only when surplus air crossed the mountains in April (Figure 4e), but the multiyear average was still negative, and there was still a dangerous possibility of the precipitation conditions causing drought.

Similarly, a bivariate spatial correlation analysis was performed for the SPI and YRR. The results of the correlation analysis showed that the spatial relationship between the SPI and wheat yield was negative. The wheat yield reduction rate was usually not high in Anyang city, which had more precipitation than other regions. The SPI had an ideal effect on the drought evaluation, and its precision even reached 0.52 (Figure 6b), indicating that regions with poor precipitation were highly correlated with regions with high wheat yield reduction rates. However, when using the SPI for drought monitoring, the same problem appears as that found with the TVDI; that is, in some years (Figure 6c and d), the spatial correlations between the other indexes were not high, especially in 2016. To some extent, the situation described above reduced the scope of the application of the SPI in drought assessments.

3.4 Validation of agricultural drought monitoring using the IDEIW

The IDEIW was used to analyze the drought intensity and spatiotemporal dynamics of drought.

After screening, 2002, 2005, 2007, 2011, 2016 and 2018 were selected as the typical years. To clearly distinguish the spatial variability in drought intensity in this study, the colors were subdivided according to the actual situation. The results showed that drought had high spatial differences among different years, and partial drought event of different degrees occurred in each year, mainly mild and moderate drought (Figure 7a); this was consistent with the results of previous studies (**Chen et al. 2017**). The years 2002 and 2018 (Figure 7a and f) were the most severe of the six years, with bright colors and high values. Moderate drought occurred in the central and northeastern districts of Anyang city in these two years. Second, in 2005 and 2011 (Figure 7b and d), disasters mainly occurred in the western and eastern margins of the study area. The lowest degree of drought was observed in 2016 (Figure 7e), but in this year, arid regions were the most widespread, with almost all growing areas affected by drought. The year 2007 was a wet year (Figure 7c) during which the main planting area was unaffected. Drought occurred frequently in the whole northern region and was the most severe in the central region (Figure 7a-f). Drought in the southeastern margin was also frequent (Figure 7b, d and f), but the intensity was usually not high.

Taking 2016 as an example, the monthly IEDEIW (Figure 7g, h and i) values showed that drought occurred mainly in the northeast and central districts of Anyang city, which manifested a tendency to spread. A continuing shortage of rainfall caused drought in March; in April, the drought began to spread westward. In May, the drought continued to spread westward, but as rainfall resumed, the severity of the disaster began to ease. On the whole, drought trended from east to west and then gradually weakened.

To verify the availability of the IDEIW in assessing agricultural drought, the YRRs of four drought years (2002, 2005, 2011 and 2016) were used to study the spatial correlation with the IDEIW. The results showed that there was a strong spatial relationship between the IDEIW and YRR in the dry years, and all correlation coefficients passed the significance test (P value < 0.05) (Figure 8). Only in 2011 (Figure 8c) was the correlation between two variables weaker than those of the others; however, it was still greater than 0.30, which constitutes a moderate correlation. In general, the drought intensity reflected by the IDEIW has a strong spatial correlation with the disaster-affected intensity reflected by the YRR, and the IDEIW can effectively identify the distinction between drought and moist conditions.

4 Discussion

4.1 Precision comparison with the monitoring of the TVDI

To understand the precision of the IDEIW in drought monitoring, the relationship between the TVDI and YRR was analyzed by using bivariate spatial correlation to compare the reduction rate with the IDEIW. In dry years, the spatial correlation between the TVDI and YRR was lower than that between the TVDI and IDEIW, which was obviously not as good as the integrated evaluation model for drought monitoring (Figures 5 and 8). There are two main reasons for this result: on the one hand, the adaptability of the TVDI is affected by vegetation and satellite quality, as shown by Yu *et al.* (**2011**) and Li *et al.* (**2014**); on the other hand, among climatic factors, precipitation and temperature, have the greatest influence on drought (**Tian et al. 2020**), but the TVDI only

406 considers surface temperature when evaluating drought. In comparison, the relationship between
407 the IDEIW and the spatial distribution of disaster-affected wheat areas is more stable than the
408 relationship between the IDEIW and TDVI, and the precision of the drought evaluation is better
409 than that of the TVDI. Therefore, the integrated evaluation model is more suitable for agricultural
410 drought monitoring than the TVDI is.
411
412 ***4.2 Sensitivity comparison with the monitoring of SPI***
413 To understand the sensitivity of the IDEIW to drought, the precipitation distribution and drought
414 evaluation results obtained with the integrated evaluation model were compared (Figure 4d-f and
415 Figure 7g-i). As can be clearly seen from the figure, the monthly IDEIW values show that the
416 distributions of dry regions and precipitation highly overlap, and the SPI numeric values of red
417 zones are usually negative. However, in the southeast region of the study area, the similarity
418 between the distributions of precipitation and arid regions is reduced (Figures 4f and 7i), and the
419 TVDI evaluation results are more similar than the SPI results to the distribution of arid regions
420 (Figures 4c and 7i). Therefore, it can be inferred that precipitation is still the most important factor
421 affecting drought but is not the only factor (**Labedzki 2007**); this result is also consistent with the
422 research results of Tian *et al.* (**2020**) on the North China Plain.
423 To further explore the relationship between the IDEIW and precipitation, the applicabilities
424 of the SPI and IDEIW were compared using the spatial distribution of the wheat yield reduction
425 rates. In 2005 and 2011, the spatial correlation between the SPI and YRR was slightly better than
426 that of the IDEIW (Figures 6b and c and 8b and c), but the precision of the SPI in the other two

years was significantly less than that of the YRR (Figures 6a and d and 8a and d). By analyzing the meteorological data, the years with excellent evaluation effects of SPI were found to all remain in extremely rainless states throughout the year. It is worth noting that 2016 was also rainless throughout the year, but the evaluation effect of using the SPI was extremely poor. This is because, with the improvement of the social production level (**Li et al. 2014**), the human influence on drought becomes increasingly obvious. By comparing the social data of the three years (Table 5), it is not difficult to see that the numeric values of various indicators are much higher in 2016 than those in other years, so 2016 shows the strongest resistance. Due to environmental variations caused by human activities, a unilateral consideration of precipitation can no longer accurately describe the degree of aridity; the results of Ma (**2007**) also confirm this fact. In conclusion, the IDEIW is more stable than the SPI in drought evaluations, and it is feasible to consider human activities using the IDEIW, appropriately improving the sensitivity and stability of actual drought monitoring.

4.3 Spatial correlation validation of IDEIW in dry years

The study shows that in dry years, the spatial relationship between the IDEIW and YRR is significantly positive, and the YRR increases with the aggregation of IDEIW attributes (**Li et al. 2017**); that is, the degree of disaster will be more serious due to the aggravation of drought, which is a consistent result with Dong *et al.* (**2015**). The IDEIW can fully consider climatic conditions, soil conditions, ecological and social development, and the function of their effects better than the TVDI or SPI can, and the IDEIW is more stable and reliable than these other factors. The precision

was slightly insufficient only in 2011 (Figure 8c), and the main reason for this result was that there was little rain throughout this whole year, and underdeveloped social productivity cannot effectively cope with this situation; these conditions appropriately reduced the assessment accuracy of the integrated evaluation model. The Integrated Drought Management Plan for Central and Eastern Europe (**IDMP CEE 2014**) pointed out that the influence of too many non-water-related factors could also exacerbate the impact of water scarcity on drought. Disaster management must be integrated across sectors, and proactive measures should also be taken to reduce vulnerability. This explains why the integrated evaluation model is more stable than the SPI. Gao *et al.* (**2011**) and Du *et al.* (**2018**) both believed that adding soil background adjustment factors could significantly improve vulnerability assessments. Liang *et al.* (**2014**) also found that the influence of the soil moisture environment on climate fluctuations and drought variations was more important than other factors in Henan. The integrated evaluation model developed in this study used the TVDI instead of the NDVI for the vulnerability assessment because the TVDI can precisely reflect the soil moisture environment to some extent. Of course, there are still many deficiencies in the study. In the construction of the integrated evaluation model, the proportion of precipitation is moderately enlarged, and the evaluation range of the TVDI is also very limited. In the next step, we plan to expand the scope of the study area and evaluate the precision and stability of the long-term monitoring of the integrated evaluation model by calculating the spatial trend rate and conducting M-K tests.

5 Conclusion

Based on the principles of natural disaster risk management, an integrated drought evaluation model was established for wheat from the four perspectives of hazards, vulnerability, exposure and resistance against disasters; further, the impact of the vulnerability of the soil ecological environment on drought was taken into consideration. The results revealed the following conclusions.

(1) On the studied time scale, the yearly IDEIW indicated that drought occurred most frequently in southwestern and northern Anyang city. At the spatial scale, arid regions shown by the monthly IDEIW values and regions with scarce precipitation overlapped to a large extent, but the distribution of drought intensity in the southeast region was similar to that of the TVDI, indicating that climate is still the main cause of drought but not the only cause.

(2) Significant positive correlations were observed between the IDEIW and YRR in dry years (P value < 0.05), and there was a strong spatial relationship between these indexes. In 2002, 2005, 2011 and 2016, Moran's I reached 0.39, 0.42, 0.31 and 0.38, respectively. The drought intensity calculated based on this integrated model had good spatial correlation with the degree of disaster effects, proving, to a certain extent, the high efficiency of this integrated model for actual drought monitoring.

(3) In terms of precision comparisons, the performance of the IDEIW in agricultural drought detection was obviously better than that of TVDI. The comparison with the SPI showed that the IDEIW is more stable than individually considering precipitation. In conclusion, under the influence of precipitation, temperature, the growing environment and human

activities, the IDEIW can realize the sensitive identification of drought intensity and accurately reflect the degree of disaster-affected areas.

Funding

This research was jointly funded by the National Nature Science Foundation of China (51779093); the Support Plan for Scientific and Technological Innovation Team of Colleges and Universities in Henan Province (17IRTSTHN026); and the Key Scientific Research Projects of Henan Province (19A170010).

Conflicts of interest

The authors have no conflicts of interest regarding the present research to declare.

Availability of data and material

all data included in this study are available upon request by contact with the corresponding author.

Author Contributions

Yanbin Li: Conceptualization, Methodology, Resources, Writing - Review & Editing, Funding acquisition, Project administration, Supervision.

Yuexiong Wang: Conceptualization, Methodology, Data Curation, Formal analysis, Validation, Visualization, Writing - Original Draft.

Daoxi Li: Validation, Project administration, Writing - Review & Editing.

Jiawei Guo: Data Curation, Writing - Original Draft.

Xuefang Du: Software (Using MATLAB), Investigation, Resources.

Xiaodong Wang: Validation, Funding acquisition, Project administration

References

1. IPCC, (2018), Summary for Policymakers, in *Global Warming of 1.5°C. An IPCC Special Report on the Impacts of Global Warming of 1.5°C Above Pre-Industrial Levels and Related Global Greenhouse Gas Emission Pathways, in the Context of Strengthening the Global Response to the Threat of Climate Change, Sustainable Development, and Efforts to Eradicate Poverty*, ed. by Masson-Delmotte V, Pörtner HO, Skea J, Zhai P, Roberts D, Shukla PR, *et al*. World Meteorological Organization, Geneva, Switzerland, pp. 1–32.
2. Qu XB, Jin LX, Wang Y and Jiang FY, (2019), Comparative analysis of multiple monitoring indexes of Hulunbeier grassland drought process in spring and summer of 2017. *Meteorol Sci Technol* **1**:163–170.
3. McKee TB, Doesken NJ and Kleist J, (1995), Drought monitoring with multiple time scales preprints, in *Proceedings of the 9th Conference on Applied Climatology*. TIB, Dallas, TX, pp 233–236.
4. Vicente-Serrano SM, Zouber A, Lasanta T and Pueyo Y, (2012), Dryness is accelerating degradation of vulnerable shrublands in semiarid Mediterranean environments. *Ecol Monogr* **82**:407–428.
5. Mehran A, Mazdiyasni O and AghaKouchak A, (2015), A hybrid framework for assessing socioeconomic drought: linking climate variability, local resilience, and demand. *J Geophys Res Atmos* **120**:7520–7533.
6. Huang W, Yang X, Li M, Zhang X, Wang M, Dai S*, et al.*, (2010), Evolution characteristics of seasonal drought in the south of China during the past 58 years based

on standardized precipitation index. *Trans Chin Soc Agric Eng* **26**:50–59.

7. Wen QZ, Sun P, Zhang Q, *et al.*, (2020), Construction of nonstationary standardized precipitation evapotranspiration index and spatial and temporal pattern of future drought in China. *Acta Geogr Sin* **75**:1465–1482.

8. Kumar KCA, Reddy GPO, Masilamani P, Turkar SY and Sandeep P, (2021), Integrated drought monitoring index: a tool to monitor agricultural drought by using time-series datasets of space-based earth observation satellites. *Adv Space Res* **67**:298–315.

9. Okada N, Tatano H, Hagihara Y, Suzuki Y, Hayashi Y, Hatayama M*, et al.*, (2004), Integrated research on methodological development of urban diagnosis for disaster risk and its applications. *Disaster Prev Res Inst Annu* **47**:1–8.

10. Zhang JQ, Okada N and Tatano H, (2006), Integrated natural disaster risk management: an integrated model and China's strategic choice. *J Nat Disasters* **1**:29–37.

11. Karamouz M, Nazif S and Ahmadi A, (2013), Development of integrated drought evaluation and monitoring system: case study of aharchay river basin. *J Hydrol Eng* **18**:897–910.

12. Crausbay S, Ramirez A, Carter S, Cross M, Hall K, Bathke D*, et al.*, (2017), Defining ecological drought for the twenty-first century. *Bull Am Meteorol Soc* **98**:2543–2550.

13. Wilson SD, Schlaepfer DR, Bradford JB, Lauenroth WK, Duniway MC, Hall SA*, et al.*, (2018), Functional group, biomass, and climate change effects on ecological drought in semiarid grasslands. *J Geophys Res Biogeosciences* **123**:1072–1085.

14. Park SY, Sur C, Lee JH and Kim JS, (2020), Ecological drought monitoring through fish

habitat-based flow assessment in the Gam river basin of Korea. *Ecol Indic* **109**:105830.

15. Wang XY, Zhao XY, Li YL and et al, (2013), Research Progress on effects of environmental factors on litter decomposition in arid and semi-arid regions. *Chin J Appl Ecol* **11**:3300–3310.

16. Zhang CH, Zhang L, Wu YJ, *et al*., (2019), Comprehensive risk assessment of grassland drought disaster in Inner Mongolia. *J Arid Land Resour Environ* **33**:115–121.

17. Xia CH, He ZH, Liang H, *et al*., (2020), Monitoring of agricultural drought in Guizhou Province based on landsat 8 in 2015. *Mod Agric Sci Technol* **10**:140–143.

18. Zhang ZH and Niu LR, (2011), Wheat strain management technology under continuous drought in autumn and winter in Anyang City. *China Agric Technol Ext* **27**:23–24.

19. Song T, Duan Z, Liu JZ, *et al.*, (2015), Comparison of algorithms for retrieving land surface temperature from landsat 8 data. *J Remote Sens* **19**:451–464.

20. Sandholt I, Rasmussen K and Andersen J, (2002), A simple interpretation of the surface temperature/vegetation index space for assessment of surface moisture status. *Remote Sens Environ* **79**:213–224.

21. Wang CZ, Mao LX, He YB, *et al.*, (2009), Application of temperature vegetation drought index (TVDI) in soil moisture retrieval in Huang-Huai-Hai Plain. *Chin J Soil Sci* **5**:998–1005.

22. Guo JP, (2015), Advances in impacts of climate change on agricultural production in China. *J Appl Meteorol Sci* **26**:105–113.

23. Wu D, Li Z, Zhu Y, Li X, Wu Y and Fang S, (2021), A new agricultural drought index for

monitoring the water stress of wheat. *Agric Water Manag* **244**:106599.

24. Allan R, Pereira L, Raes D and Smith M, (1998), *Crop Evapotranspiration-Guidelines for Computing Crop Water Requirements*. FAO Irrigation and Drainage, Rome.

25. Wei K, Zhang B, Ma SQ, *et al*., (2019), Drought evolution of spring maize and its risk regionalization in Hedong region of Gansu Province. *Agric Res Arid Areas* **37**:238–247.

26. Xu L, Abbaszadeh P, Moradkhani H, Chen N and Zhang X, (2020), Continental drought monitoring using satellite soil moisture, data assimilation and an integrated drought index. *Remote Sens Environ* **250**:112028.

27. Lu HJ, Mo XG, Meng DJ, *et al.*, (2015), Temporal and spatial evolution characteristics of meteorological drought in Northeast China under the background of climate change. *Sci Geogr Sin* **8**:1051–1059.

28. Huang WH, Yang XG, Qu HH, *et al*., (2009), Analysis of spatio-temporal characteristic on seasonal drought of spring maize based on crop water deficit index. *Trans Chin Soc Agric Eng* **8**:28–34.

29. Zhao YT, (2016), *Study on Agricultural Water Resources Utilization Strategy in Northwest Arid Area under Fragile Ecosystem*. Lanzhou University, China.

30. Yao CR, (2012), The impact mechanism of population variation on climate change in the process of Urbanization: theoretical framework and cointegration test. *Urban Stud* **10**:86–91+103.

31. Pei YS, Jiang GQ and Zhai JQ, (2013), Theoretical framework and key issues of driving mechanism of drought evolution. *Adv Water Sci* **3**:449–456.

32. Wang W, Su XS and Wang XY, (2010), Ecological risk assessment of vegetation under groundwater exploitation: a case study of Wulanao, Ordos. *J Jilin Univ (Earth Sci Ed)* **6**:1344–1352.

33. Raheem N, Cravens AE, Cross MS, Crausbay S, Ramirez A, McEvoy J*, et al.*, (2019), Planning for ecological drought: integrating ecosystem services and vulnerability assessment. *WIREs Water* **6**:e1352.

34. Galarça SP, Lima CSM, Silveira GD and Rufato ADR, (2010), Correlação de pearson e análise de trilha identificando variáveis para caracterizar porta-enxerto de *Pyrus communis* L. *Ciênc Agrotecnologia* **34**:860–869.

35. Li S, Lu P, Ma JW, *et al*., (2021), Research on industry oriented standardized statistical index system. *J China Stand* **3**:91–97.

36. Zhang L, Guo CL, Zhao LY, Zhu Y, Cao WX, Tian YC*, et al.*, (2016), Estimating wheat yield by integrating the WheatGrow and PROSAIL models. *Field Crops Res* **192**:55–66.

37. Chen HT, Duan CQ, Qu L, *et al.*, (2018), Analysis of drought characteristics of maize based on information diffusion and fractal technology. *Trans Chin Soc Agric Eng* **1**:141–148.

38. Anselin L, (1995), Local indicators of spatial association—LISA. *Geogr Anal* **27**:93–115.

39. Li ZY, Zhang JJ and Geng YH, (2017), Study on the diffusion of ecological effect of urban agglomeration in Yangtze river economic belt based on spatial relationship. *J China Agric Univ* **1**:161–171.

40. Liu Y, Yue H and Li Y, (2018), Remote sensing monitoring of spring drought in Henan

Province based on MODIS. *Agric Res Arid Areas China* **3**:218–223.

41. Sharafati A, Nabaei S and Shahid S, (2020), Spatial assessment of meteorological drought features over different climate regions in Iran. *Int J Climatol* **40**:1864–1884.

42. Liu QD, Wang AJ, Guo WY, *et al*., (1999), Circulation characteristics of summer drought in Anyang area in 1997. *Meteorol Environ Sci* **3**:25–26.

43. Chen SD, Zhang LP, Tang RX, *et al*., (2017), Spatiotemporal variation of drought in Henan Province based on spei and TVDI. *Trans Chin Soc Agric Eng* **24**:126–132.

44. Yu M, Cheng MH and Liu H, (2011), Improvement and application of land surface temperature normalized vegetation index characteristic space drought monitoring method. *Acta Meteorol Sin* **5**:922–931.

45. Li HJ, Lei YP, Li CQ, *et al.*, (2014), Spatial and temporal scale effects of land surface temperature vegetation index characteristics. *Chin J Eco-Agric China* **10**:1252–1258.

46. Tian F, Wu JJ, Liu LZ, *et al*., (2020), Spatiotemporal transfer characteristics and hot spot detection of drought in North China plain from 1901 to 2015. *J Arid Land Resour Environ* **6**:87–96.

47. Labedzki L, (2007), Estimation of local drought frequency in central Poland using the standardized precipitation index SPI. *Irrig Drain* **56**:67–77.

48. Li CX, Zhao TB and Ma ZG, (2014), Assessment of the impact of human activities on climate change in typical arid and semi-arid regions of the world based on cmip5 multi model results. *Chin Sci Bull China* **30**:2972–2988.

49. Ma ZG, (2007), Relationship between the trend of aridity in North China and the decadal

oscillation of the Pacific ocean. *Chin Sci Bull China* **10**:1199–1206.

50. Dong CY, Liu ZJ and Yang XG, (2015), Effects of different levels of drought on yield of spring maize in northern China. *Trans Chin Soc Agric Eng* **11**:157–164.

51. Kindler J and Okruszko T, (2014), Integrated drought management programme in Central and Eastern Europe (IDMP CEE). *Ann Wars Univ Life Sci Land Reclam* **46**:167–179.

52. Gao Z, Gao W and Chang NB, (2011), Integrating temperature vegetation dryness index (TVDI) and regional water stress index (RWSI) for drought assessment with the aid of LANDSAT TM/ETM+ images. *Int J Appl Earth Obs Geoinf* **13**:495–503.

53. Du T, Bui D, Nguyen M and Lee H, (2018), Satellite-based, multi-indices for evaluation of agricultural droughts in a highly dynamic tropical catchment, Central Vietnam. *Water* **10**:659.

54. Liang L, Zhao S, Qin ZH, He KX, Chen C, Luo YX*, et al.*, (2014), Drought change trend using MODIS TVDI and its relationship with climate factors in China from 2001 to 2010. *J Integr Agric* **13**:1501–1508.

Figure legends

Figure 1. Distribution of wheat-growing areas and surrounding meteorological stations

Figure 2. Perennial mean comparisons of the meteorological water supply and water deficit of wheat at a monthly scale

Figure 3. Distributions of seasonal rainfall and annual yield reduction rate from 1989 to 2018

Note: The upper part of the left horizontal axis indicates that the precipitation deviation is positive, while the lower part is negative. Value above the right horizontal axis indicate reduced production; values below the axis indicate increased production

Figure 4. Spatiotemporal variability in the TVDI and SPI at a monthly scale

Figure 5. Spatial autocorrelation analysis between TVDI and YRR in dry years

Figure 6. Spatial autocorrelation analysis between SPI and YRR in dry years

Figure 7. Spatiotemporal dynamic of drought monitoring by using IDEIW

Note: Since most result values were in the same grade, applying the Percent Clip Stretch Method to differentiate the color of images was more convenient to observe the subtle changes in the spatial distribution of drought intensity. However, comparing the changes in different is particularly necessary to combine the color depth with the numerical magnitude rather than the color depth

Figure 8. Spatial autocorrelation analysis between IDEIW and YRR in dry years

Figures

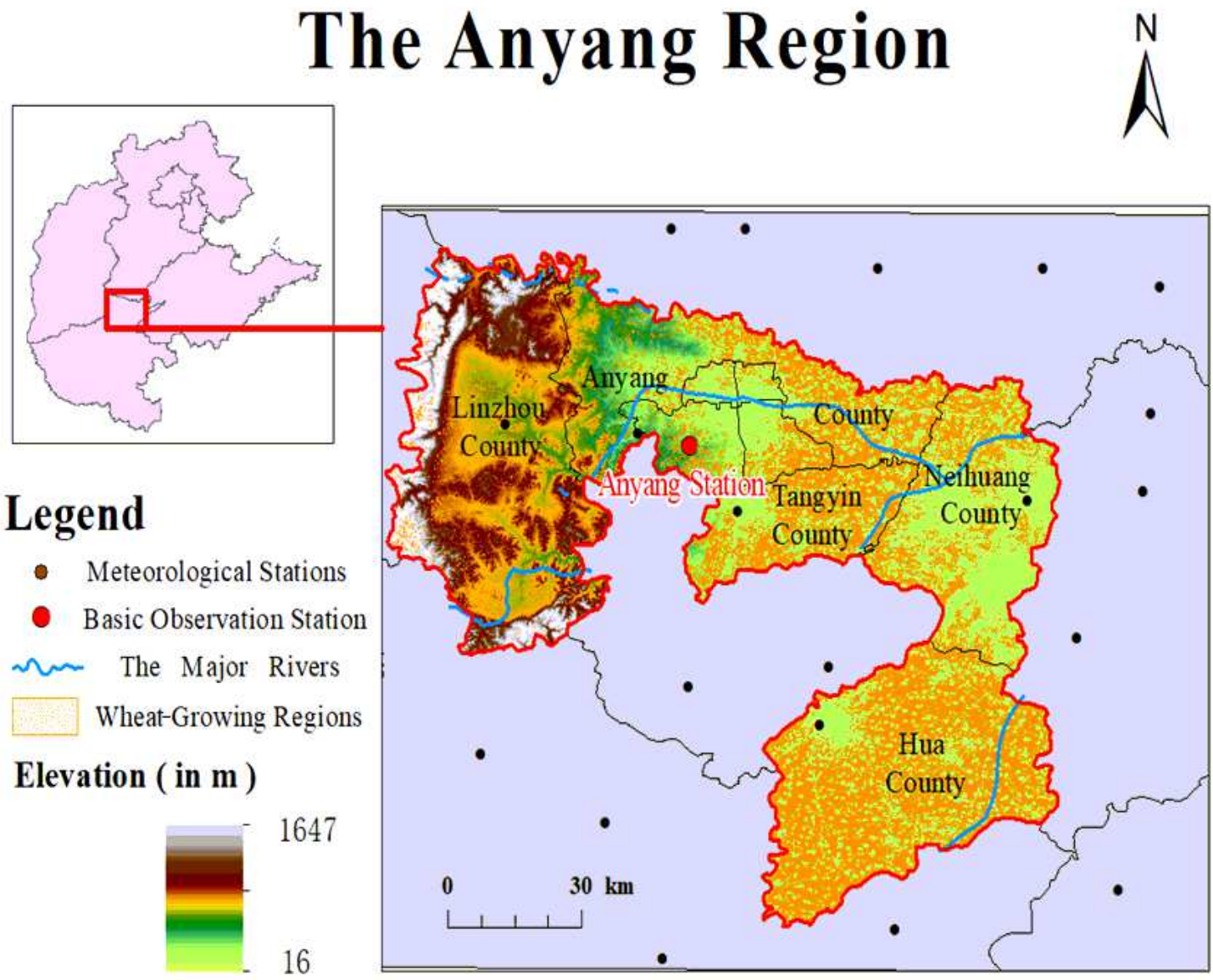

Figure 1

Distribution of wheat-growing areas and surrounding meteorological stations Note: The designations employed and the presentation of the material on this map do not imply the expression of any opinion whatsoever on the part of Research Square concerning the legal status of any country, territory, city or area or of its authorities, or concerning the delimitation of its frontiers or boundaries. This map has been provided by the authors.

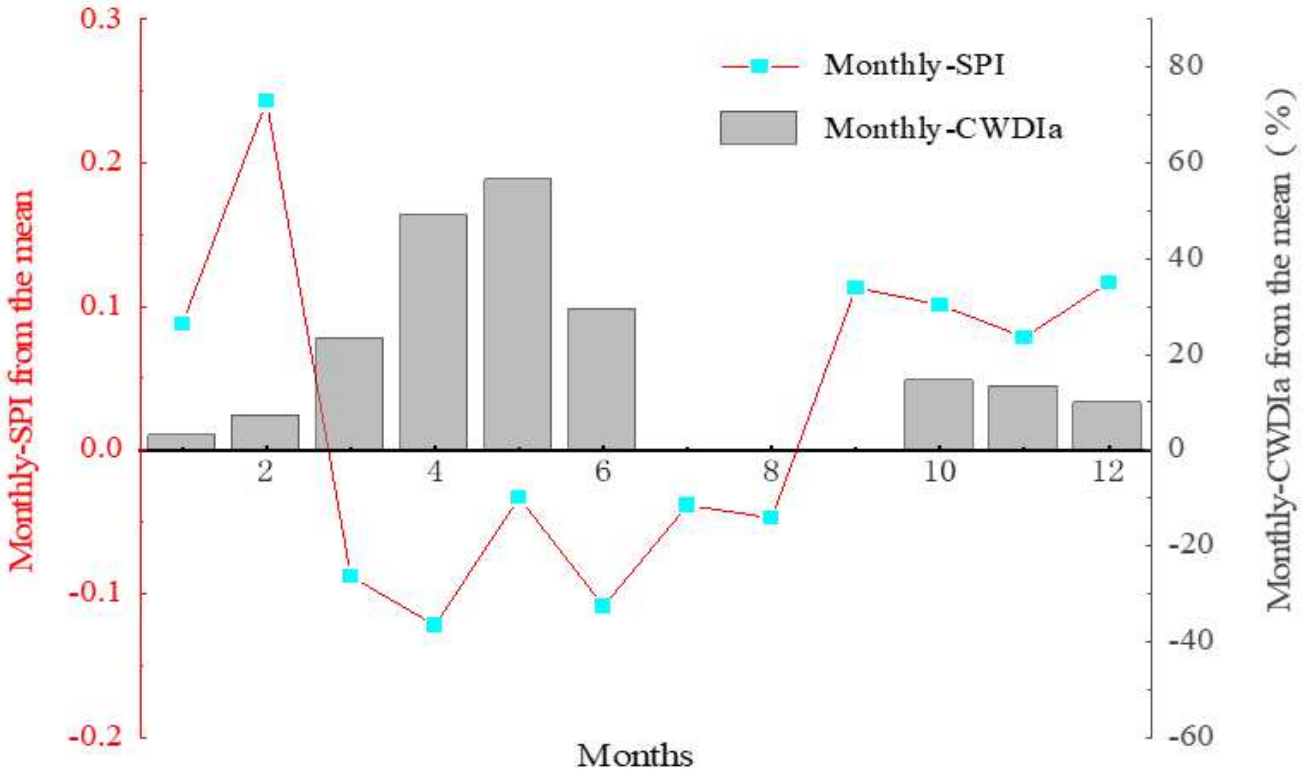

Figure 2

Perennial mean comparisons of the meteorological water supply and water deficit of wheat at a monthly scale

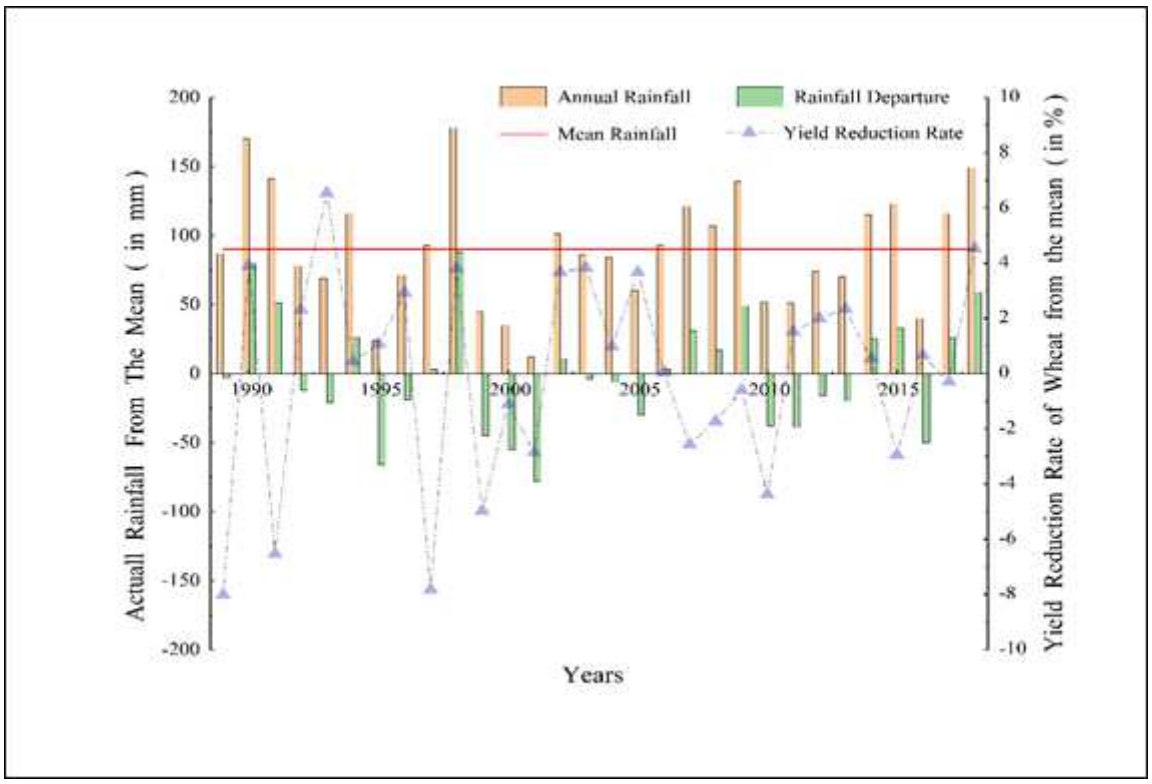

Figure 3

Distributions of seasonal rainfall and annual yield reduction rate from 1989 to 2018

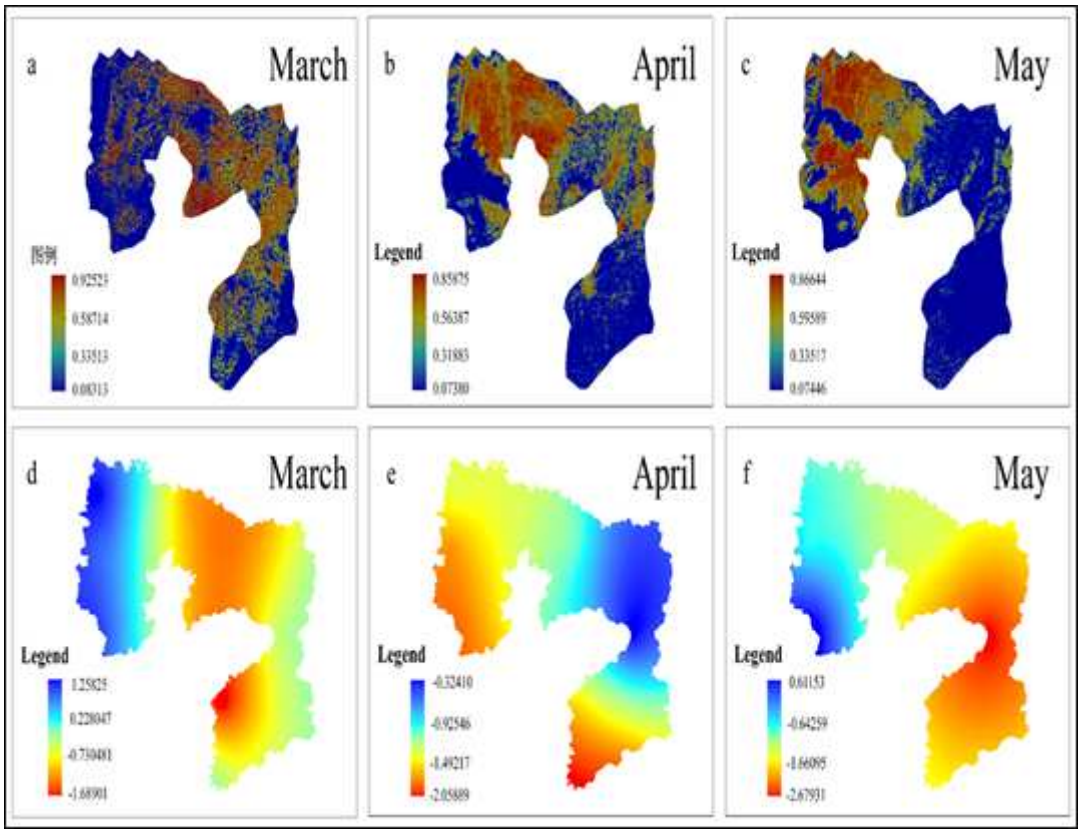

Figure 4

Spatiotemporal variability in the TVDI and SPI at a monthly scale Note: The designations employed and the presentation of the material on this map do not imply the expression of any opinion whatsoever on the part of Research Square concerning the legal status of any country, territory, city or area or of its authorities, or concerning the delimitation of its frontiers or boundaries. This map has been provided by the authors.

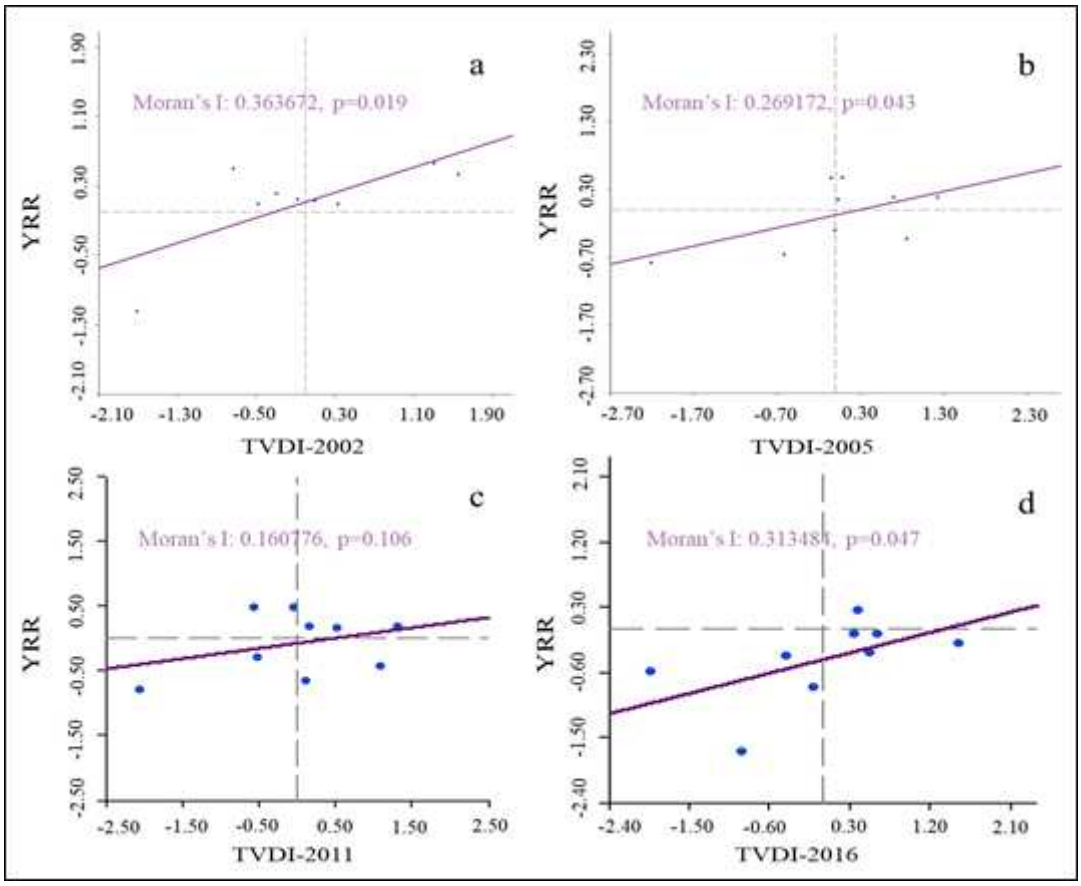

Figure 5

Spatial autocorrelation analysis between TVDI and YRR in dry years

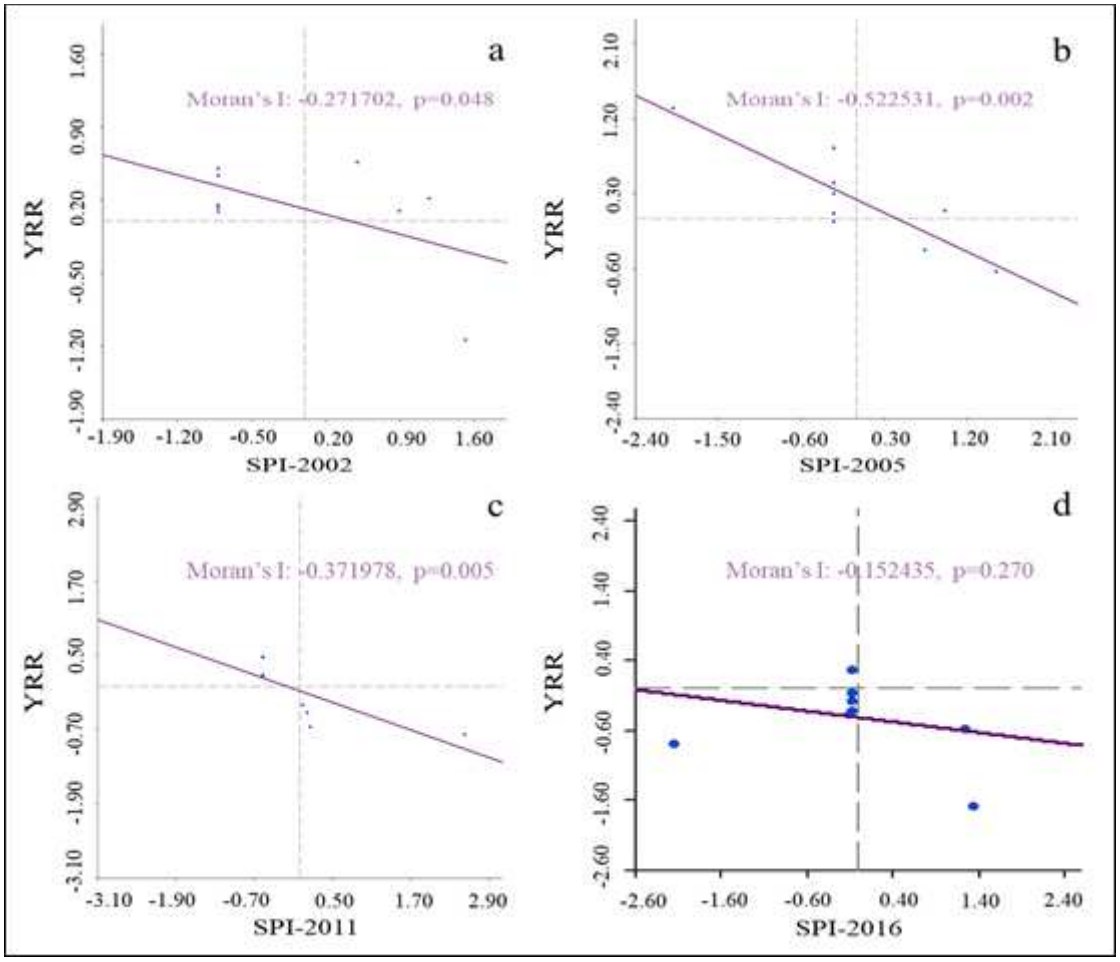

Figure 6

Spatial autocorrelation analysis between SPI and YRR in dry years

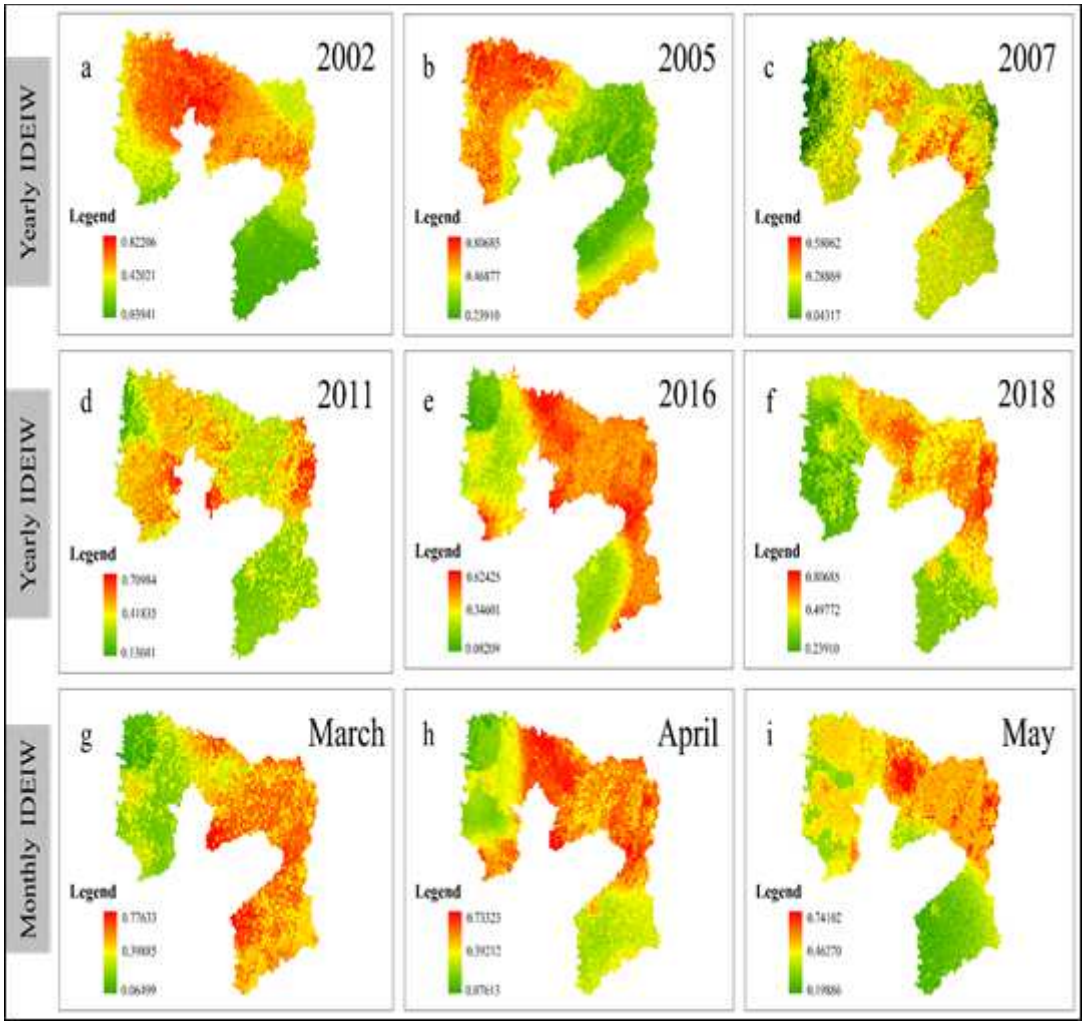

Figure 7

Spatiotemporal dynamic of drought monitoring by using IDEIW Note: The designations employed and the presentation of the material on this map do not imply the expression of any opinion whatsoever on the part of Research Square concerning the legal status of any country, territory, city or area or of its authorities, or concerning the delimitation of its frontiers or boundaries. This map has been provided by the authors.

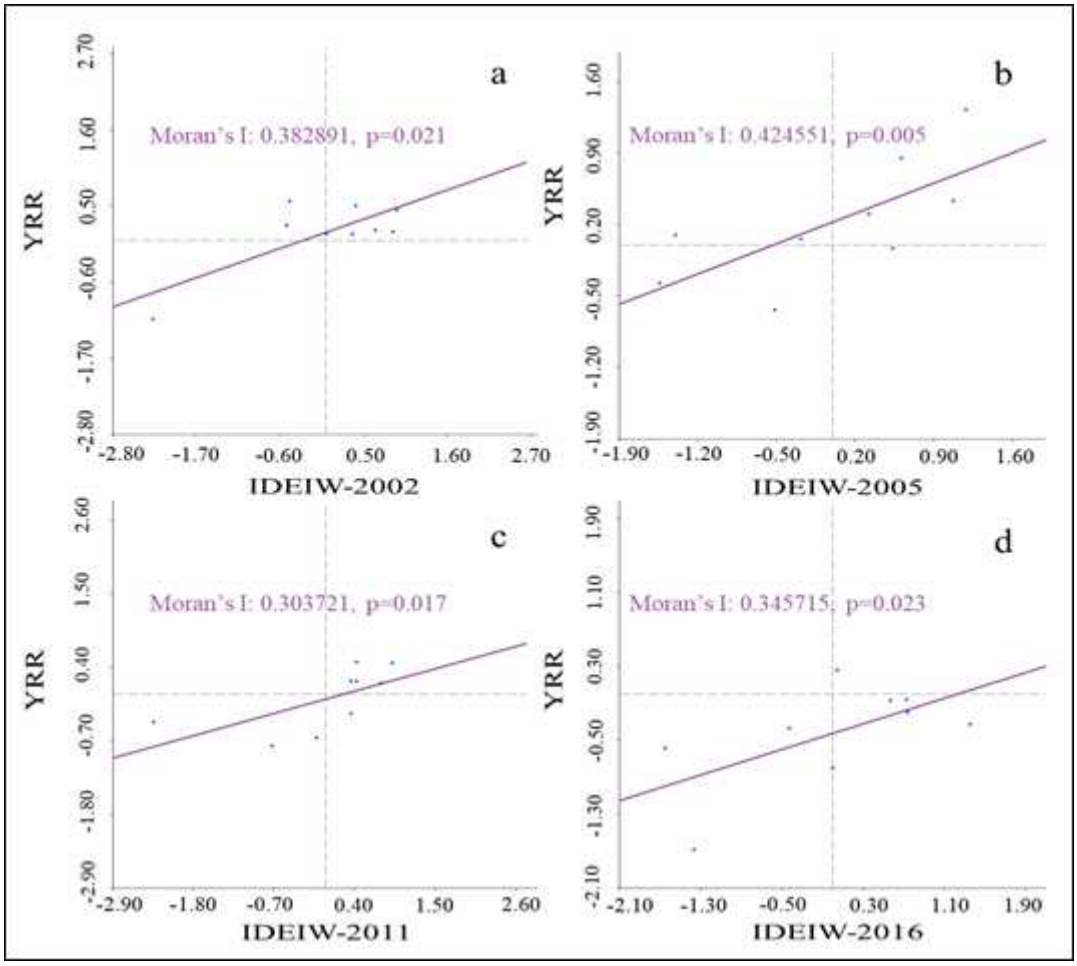

Figure 8

Spatial autocorrelation analysis between IDEIW and YRR in dry years